

Running coupling and pomeron loop effects on inclusive and diffractive DIS cross sections

M.B. Gay Ducati^{1,2}, E.G. de Oliveira³, J.T. de Santana Amaral^{4,a}

¹Instituto de Física, Universidade Federal do Rio Grande do Sul, Caixa Postal 15051, 91501-970 Porto Alegre, RS, Brazil

²CERN, PH-TH, 1211, Geneva 23, Switzerland

³Instituto de Física, Universidade de São Paulo, Caixa Postal 66318, 05315-970 São Paulo, SP, Brazil

⁴Instituto de Física e Matemática, Universidade Federal de Pelotas, Caixa Postal 354, CEP 96010-900, Pelotas, RS, Brazil

Received: 31 May 2012 / Revised: 25 September 2012 / Published online: 1 November 2012
© Springer-Verlag Berlin Heidelberg and Società Italiana di Fisica 2012

Abstract Within the framework of a $(1 + 1)$ -dimensional model which mimics high-energy QCD, we study the behavior of the cross sections for inclusive and diffractive deep inelastic γ^*h scattering cross sections. We analyze the cases of both fixed and running coupling within the mean-field approximation, in which the evolution of the scattering amplitude is described by the Balitsky–Kovchegov equation, and also through the pomeron loop equations, which include in the evolution the gluon number fluctuations. In the diffractive case, similarly to the inclusive one, suppression of the diffusive scaling, as a consequence of the inclusion of the running of the coupling, is observed.

1 Introduction

It is well known that the high-energy regime of the Quantum Chromodynamics (QCD) is described by non-linear evolution equations [1–20]. At the level of scattering amplitudes, and in the framework of the dipole picture [21–23], the most general ones are the so-called *pomeron loop equations* [24–27], which correspond to a generalization of the Balitsky–JIMWLK hierarchy [7–14, 17–20], by including the *gluon number fluctuations*. If one performs a mean-field approximation, this infinite set of equations reduces to a single closed equation for the scattering amplitude of one dipole with a hadronic target, the Balitsky–Kovchegov (BK) equation [17, 28, 29], the simplest of the non-linear equations for the scattering amplitudes in QCD at high energy. This equation admits [30–32] traveling wave solutions, which have become a natural explanation for *geometric scaling*—first observed in the HERA data for electron–proton deep inelastic scattering [33, 34]—and, being a mean-field version of

the complete hierarchy, neglects the effects of the fluctuations. At least in the fixed coupling case, from the correspondence between high-energy QCD and reaction diffusion processes, one of the consequences of the gluon number fluctuations in the evolution of the dipole scattering amplitudes is, at very high energies, the replacement of the *geometric scaling* [33, 34], by the *diffusive scaling* [35].

Fluctuation effects have not been observed in the experimental data yet. Besides, the only few phenomenological studies have been inconclusive with respect to their presence in the current experiments [36–39]. Their physical consequences in the high-energy evolution in QCD for the phenomenology were first analyzed in Ref. [35], where their effects in the behavior of inclusive and diffractive cross sections for deep inelastic lepton–hadron scattering (DIS) were studied. They found, for example, that, within the high-energy regime, all the amplitudes or cross sections show diffusive scaling, that is, they depend upon the photon virtuality Q^2 and the total rapidity Y through the variable $\ln(Q^2/\langle Q_s^2 \rangle)$, where $\langle Q_s^2 \rangle$ is the (average) hadron saturation momentum.

Our current knowledge on the consequences of the fluctuations comes only from the correspondence between high-energy QCD and statistical physics; because of the complexity of the pomeron loop equations, the properties of the solutions are known only after some approximations, in asymptotic regimes and at fixed coupling [24]. On the other hand, in the last few years one observed an important progress in the inclusion of next-to-leading order (NLO) effects in the non-linear mean-field BK equation. In particular, one can cite the explicit calculation of the running coupling effects [40–46] and its successful use in the description of HERA and RHIC data [47–49]. Unfortunately, because of the complexity of the pomeron loop equations, the inclusion of such NLO effects in these equations turn to be a very

^ae-mail: joao.amaral@ufpel.edu.br

hard task. The difficulty of dealing with these equations, even in the fixed coupling case, inspired other ways of investigation of high-energy evolution in QCD, in particular through particle models with a smaller number of dimensions [50–57]. Among them, the (1 + 1)-dimensional model presented in Ref. [55] has shown to mimic fixed impact parameter high-energy QCD with fixed coupling constant. Its generalization to the case with the running coupling was done in Ref. [56]. In such a version, the model could provide, for the first time, the study of both running coupling and fluctuations effects, taken into account simultaneously, in the high-energy evolution of scattering amplitudes. The main conclusion presented by the authors was the strong suppression of the pomeron loop (fluctuation) effects due to the running of the coupling, up to rapidity $Y \simeq 200$, that is, well beyond the energies of interest for the phenomenology in QCD. The dynamics is similar to the respective prediction of the mean-field approximation with running coupling, the property of (approximate) geometric scaling being preserved for the average scattering amplitude. This result is in sharp contrast with the fixed coupling results, which show the emergence of the diffusive scaling.

In this paper we present an investigation of the effects of both pomeron loops and running coupling, taken into account simultaneously, on the cross sections for inclusive γ^*h and, for the first time, on diffractive deep inelastic scattering (DIS), within the framework of the toy model [56]. In Sects. 2 and 3 we present some important aspects of lepton–hadron DIS, specifically an overview of kinematics and the description of the dipole picture of the inclusive and diffractive γ^*h scattering. Section 4 is devoted to an overview of the one-dimensional model in the running coupling case. In particular, we present the resulting evolution equations for the scattering amplitudes and the main features of their evolution. In Sect. 5 we present our results, with a study of the behavior of the cross sections in both fixed and running coupling cases, and the conclusions are presented in Sect. 6.

2 Inclusive virtual photon–hadron DIS

This process is described by the reaction $l(k) + h(P) \rightarrow l(k') + X(P_X)$, where l refers to the lepton (with momentum k in the initial state and k' in the final one), h to the incoming hadron (with momentum P) and X is the generic hadronic final state (with momentum P_X). Processes described by the reaction above are called *inclusive*, because only the lepton is measured in the final state. In the specific case where the lepton is an electron, its interaction with the hadron is mediated by a virtual photon with virtuality $Q^2 = -q^2 = (k - k')^2$. If one looks at $\gamma^*h \rightarrow X$, in inclusive DIS all what is known from the final hadronic state X is that it has an invariant mass squared $W^2 = (P + q)^2$,

which is the center-of-mass energy of the γ^*h system. Another important definition is that of the Bjorken variable, or Bjorken- x , given by $x_{Bj} \equiv Q^2/(Q^2 + W^2)$; from it, one sees that, for fixed values of Q^2 , when one increases the energy W^2 , x_{Bj} decreases and the high-energy limit corresponds to the small- x_{Bj} limit. The total *rapidity* of the process is defined as $Y \equiv \ln(1/x_{Bj})$.

At small- x_{Bj} , the γ^*h process can be described in a convenient frame, the so-called *dipole frame*, in which the hadron carries most of the total energy, but the virtual photon has enough energy to split into a quark–antiquark ($q\bar{q}$) pair, or a *dipole*. This dipole, then, interacts with the hadron. The dissociation of the virtual photon into the color dipole takes place long before the scattering, and the dipole evolves through soft gluon radiation until it meets the hadron (at the time of scattering) and scatters off the color fields therein. Exactly as was done in [35], the present analysis will be restricted to the leading logarithm approximation, in which the evolution consists of the emission of soft gluons, carrying a small fraction $x_{Bj} \ll 1$ of the longitudinal momentum of their parent parton. In the limit $N_c \rightarrow \infty$, a gluon can be effectively replaced by a pointlike quark–antiquark pair in a color octet state, and a soft gluon emission from a color dipole can be described as the splitting of the original dipole into two new dipoles with a common leg. In this picture, the original $q\bar{q}$ pair produced by the dissociation of the virtual photon evolves through successive dipole splittings and becomes an *onium*—i.e., a collection of dipoles—at the time of scattering. This is Mueller’s dipole picture [21–23].

Using the formalism developed in [35], one finds that the differential cross section for *onium–hadron* scattering at fixed impact parameter is given by

$$\frac{d\sigma_{\text{tot}}}{d^2b}(\mathbf{r}, \mathbf{b}, Y) = 2 \text{Re} \mathcal{A}(\mathbf{x}, \mathbf{y}, Y), \quad (1)$$

where \mathcal{A} is the amplitude for the elastic scattering, $\mathbf{b} = (\mathbf{x} + \mathbf{y})/2$ and \mathbf{r} are the impact parameter and the transverse size of the original dipole and \mathbf{x} and \mathbf{y} its transverse coordinates.

In such high-energy approximation, the DIS cross section for the inclusive *virtual photon–hadron* (γ^*h) scattering can be expressed as

$$\begin{aligned} \frac{d\sigma_{\text{tot}}^\gamma}{d^2b}(Y, Q^2) \\ = \int_0^1 dv \int d^2\mathbf{r} \sum_{\alpha=L,T} |\psi_\alpha^\gamma(\mathbf{r}, v; Q^2)|^2 2 \text{Re} \mathcal{A}(\mathbf{x}, \mathbf{y}, Y), \end{aligned} \quad (2)$$

where $|\psi_{T/L}^\gamma|^2$ are the probability densities for the $q\bar{q}$ dissociation of a virtual photon with transversal (T) or longitudinal (L) polarization, obtained from perturbative QED

[3, 58, 59], given by

$$|\Psi_T(r, v; Q^2)|^2 = \frac{2N_c\alpha_{em}}{4\pi^2} \sum_q e_q^2 \{ [v^2 + (1-v)^2] \bar{Q}_q^2 K_1^2(\bar{Q}_q r) + m_q^2 K_0^2(\bar{Q}_q r) \} \tag{3}$$

$$|\Psi_L(r, v; Q^2)|^2 = \frac{2N_c\alpha_{em}}{4\pi^2} \sum_q e_q^2 \{ 4Q^2 v^2 (1-v)^2 K_0^2(\bar{Q}_q r) \}, \tag{4}$$

where $\bar{Q}_q = v(1-v)Q^2 + m_q^2$, m_q is the mass of the quark with flavor q , $K_{0,1}$ are the McDonald functions of rank zero and one, respectively, and v is the fraction of the photon longitudinal momentum carried by the quark.

Expression (2) is a priori frame-independent, but the inclusive cross section is most simply evaluated in the frame where almost all the total rapidity Y is carried by the hadron (the target) and the projectile is an elementary dipole. In this case, $\mathcal{A}(\mathbf{x}, \mathbf{y}; Y) = \langle T(\mathbf{x}, \mathbf{y}) \rangle_Y$ [35] and

$$\frac{d\sigma_{tot}^\gamma}{d^2b}(Y, Q^2) = \int_0^1 dv \int d^2\mathbf{r} \times \sum_{\alpha=L,T} |\psi_\alpha^\gamma(v, r; Q)|^2 2\text{Re}\langle T(\mathbf{x}, \mathbf{y}) \rangle_Y, \tag{5}$$

where $\langle T(\mathbf{x}, \mathbf{y}) \rangle_Y$ is the (average) one dipole–hadron scattering amplitude, the brackets meaning the average over the target configurations. Here, we are interested in the high-energy limit of the DIS cross sections at fixed impact parameter. We assume that the dependence on \mathbf{b} can be factorized into a profile function $S(\mathbf{b})$, according to $\langle T(\mathbf{x}, \mathbf{y}) \rangle_Y = S(\mathbf{b})\langle T(r) \rangle_Y$ ($r = |\mathbf{x} - \mathbf{y}|$ is the dipole size), where the integral $\sigma_0 \equiv \int d\mathbf{b} S(\mathbf{b})$ would provide an overall normalization factor of order of the transverse area of proton. Since the dependence on \mathbf{b} in such an approximation results completely decoupled, in the following we simply set $S(\mathbf{b}) = 1$, assuming the integration over \mathbf{b} extended up to b_{max} providing the correct normalization of the cross section. The differential inclusive cross section reads

$$\frac{d\sigma_{tot}^\gamma}{d^2b}(Y, Q^2) = 4\pi \int_0^1 dv \int_0^\infty dr \times \sum_{\alpha=L,T} |\psi_\alpha^\gamma(v, r; Q)|^2 r \text{Re}\langle T(r) \rangle_Y. \tag{6}$$

As will be convenient for our purposes, we can write $\langle T(r) \rangle_Y \equiv \langle T(x) \rangle_Y \equiv \langle T_x \rangle_Y$, where $x \equiv \ln(1/r^2 Q_0^2)$ represents r in logarithmic units¹ (Q_0 is a scale of reference introduced by the initial conditions at low energy). The total cross section, then, takes the form

$$\frac{d\sigma_{tot}^\gamma}{d^2b}(Y, Q^2) = \frac{2\pi}{Q_0^2} \int_0^1 dv \int_{-\infty}^{+\infty} dx e^{-x} \times \sum_{\alpha=L,T} |\psi_\alpha^\gamma(v, x; Q)|^2 \text{Re}\langle T_x \rangle_Y. \tag{7}$$

3 Diffractive DIS

Part of the DIS events are diffractive. In such events, described by the reaction $\gamma^* h \rightarrow Xh$, the final states contain an intact scattered hadron h and a diffractive hadronic state X separated by a *rapidity gap* $Y_{gap} \equiv \ln(1/x_{\mathbb{P}})$, where $x_{\mathbb{P}} = x_{Bj}/\beta$ and β is related to the diffractive invariant mass M_X by $\beta \equiv Q^2/(Q^2 + M_X^2)$. It is straightforward to see that the difference between the total rapidity Y and the rapidity gap Y_{gap} is $Y - Y_{gap} = \ln(1/\beta)$.

The cross section for the diffractive process reads (Y_{gap} denotes the minimal rapidity gap)

$$\frac{d\sigma_{diff}^\gamma}{d^2b}(Y, Y_{gap}, Q^2) = \int_0^1 dv \int d^2\mathbf{r} \times \sum_{\alpha=L,T} |\psi_\alpha^\gamma(v, r; Q)|^2 P_{diff}(\mathbf{b}, \mathbf{r}; Y, Y_{gap}). \tag{8}$$

Since the whole process can be factorized, for our purposes it will be enough to ignore the electromagnetic process (the splitting the virtual photon into the $q\bar{q}$ dipole) and focus only on the onium–hadron ($\mathcal{O}h$) scattering. More specifically, we will be interested in the quantity P_{diff} , which is the probability for diffractive onium–hadron scattering ($\mathcal{O}h \rightarrow Xh$), and corresponds to the differential cross section for onium–hadron scattering at fixed impact parameter:

$$\frac{d\sigma_{diff}}{d^2b}(\mathbf{r}, \mathbf{b}, Y, Y_{gap}) = P_{diff}(\mathbf{x}, \mathbf{y}; Y, Y_{gap}). \tag{9}$$

An explicit formula for this probability has been obtained within the lightcone wavefunction formalism in [35], in a special frame, in which Y_{gap} coincides with the rapidity Y_0 of the target hadron. This choice of the frame is important

¹The variable x should not be confused with the bold-faced \mathbf{x} , which represents a vector in the transverse plane in the picture of DIS.

because it avoids one to deal explicitly with final state interactions. The resulting formula is given by

$$\begin{aligned}
 &P_{\text{diff}}(\mathbf{x}, \mathbf{y}; Y, Y_{\text{gap}}) \\
 &\rightarrow P_{\text{diff}}(\mathbf{x}, \mathbf{y}; Y, Y_0) \\
 &= \sum_{\{N\}} P(\{N\}; Y - Y_0) \left| \left\langle 1 - \prod_{i=1}^N S_{x_i} \right\rangle_{Y_0} \right|^2, \tag{10}
 \end{aligned}$$

which has the following meaning: starting from an original dipole (\mathbf{x}, \mathbf{y}) , after an evolution $Y - Y_0$ there is a probability density $P(\{N\}; Y - Y_0)$ for a given configuration of N dipoles to be produced. $S_{x_i} = 1 - T_{x_i}$ is the S -matrix for the scattering between the i th dipole (with logarithmic size x_i) in the projectile and a given configuration of the target, T_{x_i} being the corresponding T -matrix. The symbol $\sum_{\{N\}}$ represents the sum over all the configurations of the projectile with N dipoles. Again, the notation $\langle \cdot \rangle_{Y_0}$ denotes the average over the ensemble of color fields in the target.

Our main aim is to investigate, for the first time, the behavior of the diffractive probability (10) with increasing rapidity Y in the presence of fluctuations and running coupling effects. This requires the description of the rapidity evolution of the dipole-hadron scattering amplitude T_x , as well as the probability density $P(\{N\}; Y - Y_0)$ by taking into account both effects simultaneously, which is still a prohibitive task in full QCD. However, a convenient way of doing this is through the model presented in [56], whose main features we will briefly describe below.

4 (1 + 1)-Dimensional model for high-energy QCD

The toy model [56] is a (1 + 1)-dimensional stochastic particle model, where one of the dimensions refers to the total rapidity separation Y between two hadronic systems which undergo evolution and scattering (and plays the role of time in the evolution), while the other one (the spatial dimension) is the position of the particle along an infinite one-dimensional axis, the x -axis, which, in analogy with the dipole picture of QCD [21, 23], corresponds to the logarithm of the inverse size of a dipole, as defined in Sect. 2.

4.1 The structure of model

In this toy model, a system of particles (which corresponds to a given hadronic system) is specified by their distributions along the one-dimensional x -axis. In order to describe a scattering problem, one considers two such systems (projectile and target) which scatter off each other along a given collision axis (which is transverse to the x -axis) and assumes that each particle of the projectile can scatter elastically with any particle of the target. The total rapidity Y

of the process is divided between the right mover system (R), the projectile, which has rapidity $\delta Y \equiv Y - Y_0$ and the left mover system (L), the target, which has rapidity $-Y_0$. Let $P_R[n(x_R), Y - Y_0]$ and $P_L[m(x_L), Y_0]$ be the probability densities to find given configurations in the two systems, these being described as functions of the densities of particles at the point x . The average S -matrix is given by²

$$\begin{aligned}
 \langle S \rangle_Y &= \int \mathcal{D}n \mathcal{D}m P_R[n(x_R), Y - Y_0] \\
 &\times P_L[m(x_L), Y_0] S[n(x_R), m(x_L)]. \tag{11}
 \end{aligned}$$

Here, $S[n(x_R), m(x_L)]$ is the S -matrix associated with a given pair of configurations and the $\langle \dots \rangle$ symbol represents the average over all possible configurations $\{n(x_R)\}, \{m(x_L)\}$. This ‘event-by-event’ S -matrix is given by

$$S[n, m] = \exp \left[\int dx_R dx_L n(x_R) m(x_L) \ln \sigma(x_R|x_L) \right], \tag{12}$$

where $\sigma(x_R|x_L) = 1 - \tau(x_R|x_L)$ is the S -matrix for the scattering of two elementary particles of logarithmic sizes x_R and x_L , and $\tau(x_R|x_L)$ the corresponding T -matrix ($0 \leq \tau(x_R|x_L) \leq 1$).

The probability densities obey the following evolution equation (the details of the evolution can be found in Refs. [55, 56]):

$$\begin{aligned}
 \frac{dP[n(x), Y]}{dY} &= \int dz f_z[n(x) - \delta(x - z)] \\
 &\times P[n(x) - \delta(x - z), Y] \\
 &- \int dz f_z[n(x)] P[n(x), Y], \tag{13}
 \end{aligned}$$

where $f_z[n(x)]$ is the probability per unit rapidity to find an extra particle with logarithmic size z after an evolution step (after a small increment in rapidity, only one extra particle can be emitted), given that the initial configuration of the evolved system was $n(x)$. The functional form of the ‘deposit’ rate density $f_z[n(x)]$ can be found by assuming Lorentz invariance, and one gets

$$f_z[n(x)] = \frac{T_z[n(x)]}{\alpha(z)}, \tag{14}$$

where $T_z[n(x)]$ is the T -matrix for the scattering of a particle of logarithm size z off a system with a given configuration $n(x)$, and is given by

$$T_z[n(x)] = 1 - \exp \left[\int dx n(x) \ln \sigma(z|x) \right], \tag{15}$$

²Here we follow the same notation as used in [56].

and $\alpha(z)$ is the coupling parameter. In the case of running coupling, $\alpha(z) = 1/\beta z$ —in such a way to mimic the one-loop running coupling of QCD—, with β being the analog of the one-loop beta function of QCD. Another important feature of the model is the specification of the explicit form of the elementary particle-particle scattering amplitude $\tau(x|y)$, which, in analogy with the corresponding quantity in QCD (the amplitude for dipole–dipole scattering), is chosen as

$$\begin{aligned} \tau(x|y) &= \alpha(x)\alpha(y) \exp(-|x - y|) \\ &\equiv \alpha(x)\alpha(y)K(x, y) \equiv \alpha_x\alpha_y K_{xy}. \end{aligned} \tag{16}$$

With the above expressions at hand, one can now present the evolution equations for any observable. In particular, since we want to describe the cross section (7), we will present the resulting equations for the scattering amplitudes.

4.2 Evolution of the amplitudes

Let us consider a generic observable \mathcal{O} which depends on the configuration of the particles in the system. If one evaluates its average value at rapidity Y , one gets a measurable quantity, given by

$$\langle \mathcal{O} \rangle_Y = \int \mathcal{D}n P[n(x), Y] \mathcal{O}[n(x)], \tag{17}$$

where here we mean that the average is taken over all the configurations of the right mover, that is, $P[n(x), Y] \equiv P_R[n(x), Y]$ (the left mover consists of a given configuration of particles).

By using Eqs. (13) and (17), it is straightforward to obtain the evolution equation for any physical observable:

$$\begin{aligned} \frac{\partial \langle \mathcal{O} \rangle_Y}{\partial Y} &= \int dz \{ f_z[n(x)] \{ \mathcal{O}[n(x) - \delta(x - z)] - \mathcal{O}[n(x)] \} \}_Y. \end{aligned} \tag{18}$$

If the observable is the amplitude for the scattering between a projectile which consists of a single particle of a given logarithmic size x and a generic target, one has (the average over Y is implicit)

$$\frac{\partial \langle T_x \rangle}{\partial Y} = \alpha_x \int dz K_{xz} \langle T_z (1 - T_x) \rangle, \tag{19}$$

which is not a closed equation for $\langle T_x \rangle$, but the first equation of an infinite hierarchy. This equation is analogous to the first equation of the Balitsky–JIMWLK hierarchy, which is identical to the first of the pomeron loop (PL) equations (extended to running coupling): it has a linear term, proportional to $\langle T \rangle$, and a non-linear (quadratic) term, proportional

to T^2 . The term corresponding to the particle number fluctuations appears only in the second equation of the hierarchy, which reads

$$\begin{aligned} \frac{\partial \langle T_x T_y \rangle}{\partial Y} &= \alpha_x \int dz K_{xz} \langle T_z T_y (1 - T_x) \rangle \\ &+ \alpha_y \int dz K_{yz} \langle T_z T_x (1 - T_y) \rangle \\ &+ \alpha_x \alpha_y \int dz \alpha_z K_{xz} K_{yz} \langle T_z (1 - T_x) (1 - T_y) \rangle, \end{aligned} \tag{20}$$

the fluctuation term being the one proportional to $\langle T \rangle$ in the second line of the above equation.

In the mean-field approximation (MFA), the whole hierarchy reduces to a single closed equation, which is obtained by making $\langle TT \rangle = \langle T \rangle \langle T \rangle$ in Eq. (19), resulting in the analogous to the (running coupling) Balitsky–Kovchegov (BK) equation

$$\frac{\partial \langle T_x \rangle}{\partial Y} = \alpha_x \int_z K_{xz} [\langle T_z \rangle - \langle T_z \rangle \langle T_x \rangle]. \tag{21}$$

The evolution equations with fixed coupling can be straightforwardly obtained by simply making $\alpha = \text{constant}$. Now, we will make a brief review of the main aspects of the evolution of the average amplitude $\langle T \rangle$, in both fixed and running coupling cases.

(i) Fixed coupling case [55]:

1. From the similarity with the BK equation, Eq. (21) admits the so-called traveling wave solutions, which means that, at very large values of rapidity, the amplitude depends on x and Y through the scaling variable $x - x_s(Y)$, that is, the amplitude T is a front which interpolates between 1 and 0 and, as Y increases this front gets simply translated towards larger values of x , without being distorted. The function $x_s(Y)$ is the *saturation scale*, which naturally emerges from the non-linear evolution; it separates between the dense target region, $x \lesssim x_s$, where $T = 1$, and the dilute target region, $x \gtrsim x_s$, where T decreases exponentially. It is also an increasing function of rapidity, analogous to the (logarithm of the) saturation momentum which emerges from the non-linear evolution in QCD, $\ln(Q_s^2/Q_0^2)$. It can be also defined as the position of the front, that is, the line along which the amplitude is constant and of $\mathcal{O}(1)$ (it is usual to choose $T(x = x_s(Y), Y) = 1/2$). The dependence on the combined variable $x - x_s$ is the so-called *geometric scaling* [33, 34], which is valid in a window which grows with increasing rapidity like $\propto Y^{1/2}$.

2. With the inclusion of the fluctuation effects, the differences with respect to the mean-field analysis are very significant. From a given initial condition (at $Y = 0$), the evolution up to Y generates a statistical ensemble of fronts, which have the same form, but differ from each other by their respective front positions x_s , and this position is now a random variable. In the fixed coupling case, to a very good approximation, the distribution of x_s with Y is a Gaussian, with both the expectation value $\langle x_s \rangle$ and the dispersion σ^2 rising linearly with Y . The individual fronts exhibit geometric scaling, but only over a compact region, in contrast with the mean-field amplitude, for which the scaling window is ever increasing with Y . The average amplitude $\langle T \rangle$ is obtained by averaging over the ensemble, and one gets that the geometric scaling property of the individual fronts is washed out by the dispersion of the fronts, and is replaced, at sufficiently large Y , by *diffusive scaling*.

(ii) Running coupling case [56]:

1. In the MFA, geometric scaling is also present at asymptotic rapidities in the evolution of the amplitude, but the front formation is delayed in comparison with the fixed coupling case: the window for geometric scaling grows with increasing rapidity like $\propto Y^{1/6}$.
2. After the inclusion of the fluctuations, the growth of the dispersion with Y is suppressed, and one has $\sigma^2 \propto \sqrt{Y}$. Besides, the influence of the fluctuations is strongly suppressed, remaining negligible for all the rapidities of interest. In particular, the average amplitude exhibits *approximate* geometric scaling: the deviation from geometric scaling with increasing Y is too small.

5 Results

Now we can study the consequences of the properties of the scattering amplitudes discussed above on the behavior of the

cross section (7) and the diffractive probability (10) with increasing Y . Concerning the inclusive cross section (7), our aim here is only to reproduce the results obtained in [35] and [56], respectively, at fixed and running coupling. The diffractive case is our main result: in the high-energy limit, it has been shown that, in the fixed coupling case, diffractive cross section exhibits diffusive scaling [35]. Here, for the first time, we study the behavior of this quantity with increasing energy in the presence of both fluctuation and running coupling effects.

For the purposes cited above, we must use as the input for the average scattering amplitude for particle–hadron (dipole–hadron) the solution of Eq. (19) (when fluctuations are included) and (21) (when fluctuations are not included, that is, in the MFA). The parameters which enter into the expression for the cross section (7) must be fixed: we set $Q_0^2 = 1 \text{ GeV}^2$, the electromagnetic coupling constant $\alpha_e = 1/137$, the number of colors $N_c = 3$, and only light quarks (u, d, s) enter into this analysis, with zero masses. In both inclusive and diffractive cases, we perform the analysis first considering the fixed coupling case, in both mean-field approximation (MFA) and with fluctuations included and then we generalize it by doing the same in the case with running coupling. In the specific case of diffractive onium–hadron scattering, in the evaluation of the probabilities $P(\{N\}; \delta Y)$ for a given configuration of the projectile onium at rapidity δY , as well as the averages over all the target configurations, we follow the same procedure as described in [55].

5.1 Fixed coupling case

The results in the case of fixed coupling (FC) are shown in Figs. 1 and 2. The value of the coupling constant is chosen to be $\alpha = 0.2$. Figure 1 presents the DIS inclusive cross section as a function of the variable $Q^2/\langle Q_s^2 \rangle$, for different values of rapidity, up to $Y = 100$. One should remember that the average saturation momentum, $\langle Q_s^2(Y) \rangle$, is related to the average saturation scale $\langle x_s(Y) \rangle$: $\langle x_s(Y) \rangle = \ln(\langle Q_s^2(Y) \rangle / Q_0^2) = \ln(1/\langle r_s \rangle^2 Q_0^2)$. In the MFA (left plot), one clearly sees the geometric scaling, as well as the growth of its window as rapidity increases from $Y = 0$. For values of rapidity values

Fig. 1 Fixed coupling results for various rapidities as a function of $Q^2/\langle Q_s^2 \rangle$, in the MFA (left plot) and with the inclusion of the fluctuations (right plot), up to rapidity $Y = 100$

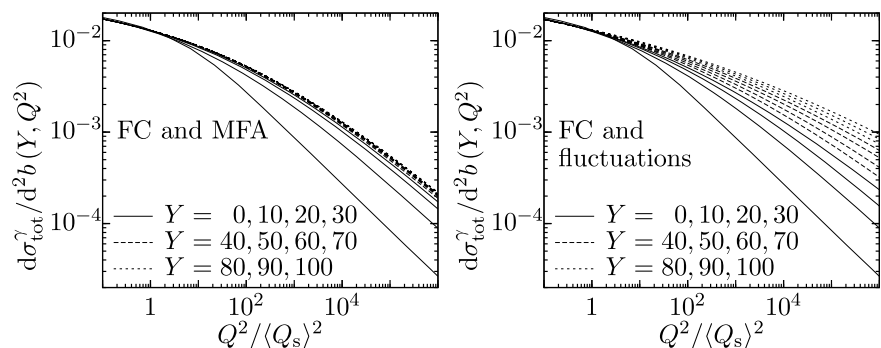


Fig. 2 Diffractive probability for onium–hadron scattering as a function of the scaling variable $\langle r_s^2 \rangle / r^2$: fixed coupling results for various rapidities, in the MFA (left plot) and with fluctuations (right plot), up to rapidity $Y = 95$

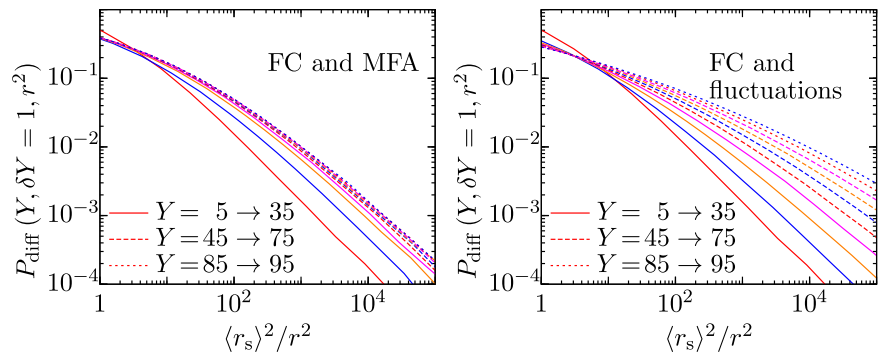
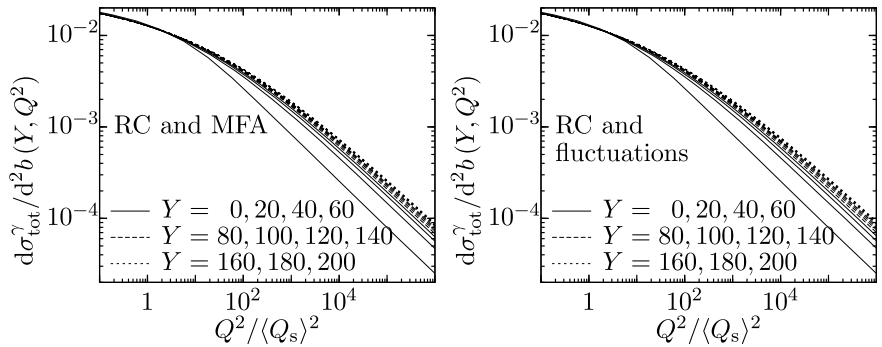


Fig. 3 Running coupling results for various rapidities as a function of $Q^2 / \langle Q_s^2 \rangle$, in the MFA (left plot) and with the inclusion of the fluctuations (right plot), up to rapidity $Y = 200$



$Y \gtrsim 30$, the curves for the cross section have the same shape and they depend only on the scaling variable $Q^2 / \langle Q_s^2 \rangle$. After the inclusion of the fluctuations (right plot), the curves deviate from the mean-field behavior (and thus from geometric scaling) as Y increases. These FC results for the inclusive cross section reflect the corresponding behavior of the scattering amplitude and are consistent with the ones already obtained in the QCD framework [35].

In Fig. 2 the diffractive probability for onium–hadron DIS is shown as a function of the geometric scaling variable $\langle r_s^2 \rangle / r^2 = e^{-((x_s) - x)}$ for different values of the total rapidity interval Y . The rapidity interval of the projectile onium, $\delta Y = Y - Y_0$, is kept fixed at a small value ($\delta Y = 1$), to ensure that the projectile is a dilute system, consisting of a small number of particles (dipoles). In the MFA, geometric scaling is reached at very large values of Y . When fluctuations are included, one observes that, similarly to the inclusive cross section, geometric scaling breaks down and P_{diff} exhibits diffusive scaling. This result is consistent with what has been found in [35].

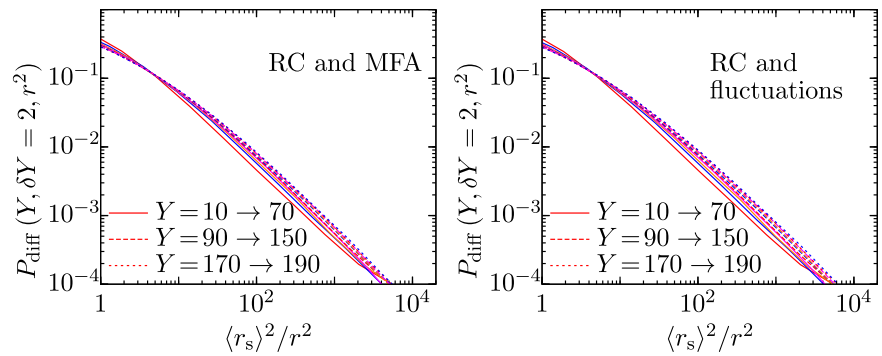
5.2 Running coupling case

Now, we proceed with a generalization of the previous case, by taking into account the running of the coupling, given by $\alpha_x = 1/\beta x$, with β chosen to be 0.72. The results are shown in Fig. 3, where the cross section (7) is represented as a function of the variable $Q^2 / \langle Q_s^2 \rangle$, for different values of rapidity,

up to $Y = 200$. In the MFA, one can observe geometric scaling, but it is reached at larger values of rapidity in comparison with the FC case. This reflects the corresponding behavior of the scattering amplitude, for which the formation of the front in the RC case is delayed. With the inclusion of the fluctuations, one can observe that the increasing dispersion present in the FC case is strongly suppressed and one has an approximate geometric scaling, since the different curves have quite small deviations from each other when increasing rapidity, resulting in a behavior very similar to the MFA (with running coupling). Then, the high-energy behavior of the inclusive cross section reflects the corresponding behavior of the average particle (dipole) scattering amplitude in the running coupling case, as expected.

Our next step is to investigate if the suppression obtained in the inclusive case, due to both fluctuation and running coupling effects, holds also for the diffractive probability $P_{\text{diff}}(r, Y, \delta Y)$. This answer is the main result of this paper. First, from the left plot in Fig. 4 we can see that, in the MFA, geometric scaling is observed, as expected, but is reached faster than in the FC case, at smaller values of rapidity (now $\delta Y = 2$). Finally, in the right plot we present, for the first time, a study of the behavior of the diffractive probability in the presence of both fluctuation and RC effects. Suppression of fluctuations exists and is as strong as in the MFA case. Therefore, in diffractive DIS, within the framework of the toy model for high-energy QCD, fluctuations are strongly suppressed by the running of the coupling

Fig. 4 Diffractive probability for onium–hadron scattering as a function of the scaling variable $\langle r_s^2 \rangle / r^2$: running coupling results for various rapidities, in the MFA (left plot) and with fluctuations (right plot), up to rapidity $Y = 190$



and diffusive scaling of the cross sections, predicted in the FC case, is washed out.

6 Conclusions

In this paper we have investigated the high-energy behavior of the total cross section for virtual-photon–hadron DIS and for onium–hadron diffractive DIS within the framework of the $(1 + 1)$ -dimensional model [56], which provides a way to study, at fixed impact parameter, the effects of the particle number fluctuations and running coupling, taken into account simultaneously. In the fixed coupling case, the results are consistent with those obtained in the framework of QCD [35], that is, the geometric scaling which is present in the mean-field approximation at large values of rapidity, is completely washed out when fluctuations are taken into account.

By generalizing the analysis done in [35], through the inclusion of running coupling effects, we have reproduced the results obtained in [56] for the inclusive virtual photon–hadron cross section: the behavior of this cross section with and without fluctuations is similar, this observable presenting approximate geometric scaling, which means that the running of the coupling suppresses the fluctuation effects at asymptotic rapidities. In the diffractive onium–hadron scattering, the diffractive probability exhibits geometric scaling in the MFA. When fluctuations are included, diffusive scaling is seen in the fixed coupling case, while that, in the running coupling case, geometric scaling is present and reached at smaller values of rapidity Y than in the case without fluctuations.

This suggests that the mean-field treatment with running coupling would be enough to study not only the inclusive lepton–hadron DIS, but also the diffractive DIS, for all the energies available at present and to be available in a near future. The toy model also allows the investigation of the other processes which, in the framework of QCD, admit a dipole factorization. Thus, it would be interesting to apply it to such processes, in particular less inclusive ones, in order to investigate if the suppression of fluctuations by running coupling effects remains present.

Acknowledgements We would like to thank Andrea Beraudo and Yuri Kovchegov for very useful discussions. M.B.G.D. acknowledges the hospitality of the CERN Theoretical Division and J.T.S.A. acknowledges the hospitality of GFPAE-IF-UFRGS. This work has been supported by CNPq and FAPERGS (Brazil). E.G.O. is supported by FAPESP (Brazil) under contract 2011/50597-8.

References

1. L.V. Gribov, E.M. Levin, M.G. Ryskin, Phys. Rep. **100**, 1 (1983)
2. A.H. Mueller, J. Qiu, Nucl. Phys. B **268**, 427 (1986)
3. A.H. Mueller, Nucl. Phys. B **335**, 115 (1990)
4. A.L. Ayala, M.B.G. Ducati, E.M. Levin, Nucl. Phys. B **493**, 305 (1997)
5. A.L. Ayala, M.B.G. Ducati, E.M. Levin, Nucl. Phys. B **551**, 335 (1998)
6. A.L. Ayala, M.B.G. Ducati, E.M. Levin, Phys. Lett. B **388**, 188 (1996)
7. J. Jalilian-Marian, A. Kovner, A. Leonidov, H. Weigert, Nucl. Phys. B **504**, 415 (1997)
8. J. Jalilian-Marian, A. Kovner, A. Leonidov, H. Weigert, Phys. Rev. D **59**, 014014 (1999)
9. J. Jalilian-Marian, A. Kovner, H. Weigert, Phys. Rev. D **59**, 014015 (1999)
10. A. Kovner, J.G. Milhano, H. Weigert, Phys. Rev. D **62**, 114005 (2000)
11. E. Iancu, A. Leonidov, L. McLerran, Nucl. Phys. A **692**, 583 (2001)
12. E. Iancu, A. Leonidov, L. McLerran, Phys. Lett. B **510**, 133 (2001)
13. E. Ferreira, E. Iancu, A. Leonidov, L. McLerran, Nucl. Phys. A **703**, 489 (2002)
14. E. Iancu, L. McLerran, Phys. Lett. B **510**, 145 (2001)
15. N. Armesto, M. Braun, Eur. Phys. J. C **20**, 517 (2001)
16. N. Armesto, M. Braun, Eur. Phys. J. C **22**, 351 (2001)
17. I. Balitsky, Nucl. Phys. B **463**, 99 (1996)
18. I. Balitsky, Phys. Lett. B **518**, 235 (2001)
19. I. Balitsky, Phys. Rev. Lett. **81**, 2024 (1998)
20. H. Weigert, Nucl. Phys. A **703**, 823 (2002)
21. A.H. Mueller, Nucl. Phys. B **415**, 373 (1994)
22. A.H. Mueller, B. Patel, Nucl. Phys. B **425**, 471 (1994)
23. A.H. Mueller, Nucl. Phys. B **437**, 107 (1995)
24. E. Iancu, D.N. Triantafyllopoulos, Nucl. Phys. A **756**, 419 (2005)
25. A.H. Mueller, A.I. Shoshi, S.M.H. Wong, Nucl. Phys. B **715**, 440 (2005)
26. E. Iancu, D.N. Triantafyllopoulos, Phys. Lett. B **610**, 253 (2005)
27. E. Levin, M. Lublinsky, Nucl. Phys. A **763**, 172 (2005)

28. Yu.V. Kovchegov, Phys. Rev. D **60**, 034008 (1999)
29. Yu.V. Kovchegov, Phys. Rev. D **61**, 074018 (1999)
30. S. Munier, R. Peschanski, Phys. Rev. Lett. **91**, 232001 (2003)
31. S. Munier, R. Peschanski, Phys. Rev. D **69**, 034008 (2004)
32. S. Munier, R. Peschanski, Phys. Rev. D **70**, 077503 (2004)
33. A.M. Stasto, K. Golec-Biernat, J. Kwiecinski, Phys. Rev. Lett. **86**, 596 (2001)
34. C. Marquet, L. Schoeffel, Phys. Lett. B **639**, 471 (2006)
35. Y. Hatta, E. Iancu, C. Marquet, G. Soyez, D.N. Triantafyllopoulos, Nucl. Phys. A **773**, 95 (2006)
36. M. Kozlov, A. Shoshi, W. Xiang, J. High Energy Phys. **0710**, 020 (2007)
37. E. Basso, M.B. Gay Ducati, E.G. de Oliveira, J.T. de Santana Amaral, Eur. Phys. J. C **58**, 9 (2008)
38. W. Fischer, Front. Phys. China **6**, 100 (2011)
39. V.P. Gonçalves, J.T. de Santana Amaral, Phys. Rev. D **86**, 054019 (2012)
40. Y.V. Kovchegov, H. Weigert, Nucl. Phys. A **784**, 188 (2007)
41. Y.V. Kovchegov, H. Weigert, Nucl. Phys. A **789**, 260 (2007)
42. J.L. Albacete, Y.V. Kovchegov, Phys. Rev. D **75**, 125021 (2007)
43. I. Balitsky, Phys. Rev. D **75**, 014001 (2007)
44. I. Balitsky, G.A. Chirilli, Phys. Rev. D **77**, 014019 (2008)
45. Y.V. Kovchegov, J. Kuokkanen, K. Rummukainen, H. Weigert, Nucl. Phys. A **823**, 47 (2009)
46. Y.V. Kovchegov, Phys. Lett. B **710**, 192 (2012)
47. J.L. Albacete, N. Armesto, J.G. Milhano, C.A. Salgado, Phys. Rev. D **80**, 034031 (2009)
48. M.A. Betemps, V.P. Gonçalves, J.T. de Santana Amaral, Eur. Phys. J. C **66**, 137 (2010)
49. J.L. Albacete, N. Armesto, J.G. Milhano, P. Quiroga-Arias, C.A. Salgado, Eur. Phys. J. C **71**, 1705 (2011)
50. P. Rembiesa, A.M. Stasto, Nucl. Phys. B **725**, 251 (2005)
51. A. Kovner, M. Lublinsky, Nucl. Phys. A **767**, 171 (2006)
52. A.I. Shoshi, B.-W. Xiao, Phys. Rev. D **73**, 094014 (2006)
53. M. Kozlov, E. Levin, Nucl. Phys. A **779**, 142 (2006)
54. J.-P. Blaizot, E. Iancu, D.N. Triantafyllopoulos, Nucl. Phys. A **784**, 227 (2007)
55. E. Iancu, J.T. de Santana Amaral, G. Soyez, D.N. Triantafyllopoulos, Nucl. Phys. A **786**, 131 (2007)
56. A. Dumitru, E. Iancu, L. Portugal, G. Soyez, D.N. Triantafyllopoulos, J. High Energy Phys. **0708**, 062 (2007)
57. S. Munier, G.P. Salam, G. Soyez, Phys. Rev. D **78**, 054009 (2008)
58. N.N. Nikolaev, B.G. Zakharov, Z. Phys. C **49**, 607 (1991)
59. N.N. Nikolaev, B.G. Zakharov, Z. Phys. C **53**, 331 (1992)